(e) of Fig. 5 show the behavior of the $\phi = \pi/2$ cut of the radiated field for the following anisotropic slabs: sapphire (Fig. 4); Epsilam-10 (Fig. 5(a)); pyrolitic boron nitride (Fig. 5(b)); and biaxial materials ((c)–(e) of Fig. 5).

The numerical computations have shown, in the case of an electric $\hat{z}$-oriented point source, that the radiated patterns present a symmetry with respect to the vertical axis ($\theta = \pi/2$) and a phenomenon of crouching of the radiation maxima that progressively widen towards the radiation region on the horizon plane ($\theta = 0, \pi$), reaching it when (45) holds. The radiated patterns depend not on ϵ_{xx}, μ_{yy}, μ_{zz} but only on the parameters d, h, ϵ_{yy}, ϵ_{zz}, μ_{xx}. Finally, we observe that the electric far field in the $\phi = \pi/2$ cut sustained by an electric $\hat{x}$-oriented point source depends on the $\tilde{G}_{xx}$ term and, therefore, on the parameters ϵ_{xx}, μ_{yy}, μ_{zz}.

V. Conclusion

In this paper we have studied the circuit modeling of a planar structure with a general anisotropic slab by using a transmission-line analogy. This important result has been found: when the constitutive parameters assume the double or simple diagonal form, circuit modelization is always possible. For $\underline{\epsilon}$ and $\underline{\mu}$ of a more general form, this circuit representation is still possible, provided that the constitutive tensors have the same principal coordinates. Moreover, we have applied this result to two study cases: 1) the unbounded gyrotropic medium, vertically polarized, described by the double diagonal tensors $\underline{\epsilon}$ and $\underline{\mu}$ and 2) the biaxial anisotropic grounded slab embedded in an unbounded isotropic half-space, fed by an electric planar deep point source. Case 2) has been extensively investigated by deriving in a closed analytical form the spectral (Fourier) dyadic Green function of the structure and by obtaining important information on the properties of radiation of the structure together with conditions to control the radiation on the horizon plane.

Finally, numerical evaluations of planar structure radiated fields, backed with a slab of different anisotropic material, have been presented along with important information on the electromagnetic constants of the medium, the thickness of the slab, the position of the source, and the working frequency.

References

[1] J. A. Kong, "Electromagnetic fields due to dipole antennas over stratified anisotropic media," *Geophys.*, vol. 37, pp. 958–966, Dec. 1972.

[2] H. C. Chen, *Theory of Electromagnetic Waves.* New York: McGraw-Hill, 1983.

[3] C. M. Krowne, "Green's function in the spectral domain for biaxial and uniaxial anisotropic planar dielectric structures," *IEEE Trans. Antennas Propagat.*, vol. 32, pp. 1273–1281, Dec. 1984.

[4] C. M. Krowne, "Determination of the Green's function in the spectral domain using a matrix method: Application to radiators or resonators immersed in a complex anisotropic layered medium," *IEEE Trans. Antennas Propagat.*, vol. 34, pp. 247–253, Feb. 1986.

[5] C. M. Krowne, "Electromagnetic theorems for complex anisotropic media," *IEEE Trans. Antennas Propagat.*, vol. 32, pp. 1224–1230, Nov. 1984.

[6] M. N. Afsar, "Dielectric measurements of millimeter-wave materials," *IEEE Trans. Microwave Theory Tech.*, vol. 32, pp. 1598–1609, 1984.

[7] M. Soinski, Z. Bak, and P. Braigel, "Anisotropy of magnetic properties in thin electrical sheets," *IEEE Trans. Magn.*, vol. 26, pp. 3076–3079, Nov. 1990.

[8] A. Lakhtakia, V. K., and V. V. Varadan, "Reflection and transmission of plane waves at the planar interface of a general uniaxial medium and free space," *J. Modern Optics*, vol. 38, no. 4, pp. 649–657, Apr. 1991.

[9] J. L. Tsalamengas and N. K. Uzunoglu, "Radiation from a dipole in the proximity of a general anisotropic grounded layer," *IEEE Trans. Antennas Propagat.*, vol. 33, pp. 165–172, Feb. 1985.

[10] J. L. Tsalamengas, "Electromagnetic fields of elementary dipole antennas embedded in stratified general gyrotropic media," *IEEE Trans. Antennas Propagat.*, vol. 37, pp. 399–403, Mar. 1989.

[11] J. L. Tsalamengas and N. K. Uzunoglu, "Radiation from a dipole near a general anisotropic layer," *IEEE Trans. Antennas Propagat.*, vol. 38, pp. 9–16, Jan. 1990.

[12] T. Itoh and W. Menzel, "A full-wave analysis method for open microstrip structures," *IEEE Trans. Antennas Propagat.*, vol. 29, pp. 63–68, Jan. 1981.

[13] L. Vegni, R. Cicchetti, and P. Capece, "Spectral dyadic Green's function formulation for planar integrated structures," *IEEE Trans. Antennas Propagat.*, vol. 36, pp. 1057–1065, Aug. 1988.

[14] R. Milo Rouselle, A. Toscano, and L. Vegni, "Transmission-line representation of planar gyrotropic structures," in *Proc. 3rd Int. Symp. Recent Advances in Microwave Technology (ISRAMT '91)* (Reno, NV), Aug. 18–21, 1991, pp. 28–31.

[15] A. Toscano and L. Vegni, "Spectral dyadic Green's function formulation for planar integrated structures with a grounded chiral slab," *J. Electromagnetic Waves Appl.* (Special Issue on Wave Interactions with Chiral and Complex Media), vol. 6, no. 5/6, pp. 751–769, 1992.

[16] H. Y. Yang, J. A. Castaneda and N. G. Alexopoulos, "Surface wave modes of printed circuit on ferrite substrates," *IEEE Trans. Microwave Theory Tech.*, MTT-40, pp. 613–620, Apr. 1992.

[17] G. Tyras, *Radiation and Propagation of Electromagnetic Waves.* New York: Academic, 1969.

[18] A. Toscano and L. Vegni, "Radiated fields from an uniaxial anisotropic grounded slab fed by a pulse source," in *1991 IEEE AP-S Int. Symp. Dig.* (London, Ontario, Canada), June 24–28, 1991, pp. 1394–1397.

[19] N. G. Alexopoulos, "Integrated-circuit structures on anisotropic substrates," *IEEE Trans. Microwave Theory Tech.*, vol. 33, pp. 847–881, Oct. 1985.

[20] R. F. Harrington and A. T. Villeneuve, "Reciprocity relations for gyrotropic media," *IRE Trans. Microwave Theory Tech.*, vol. 6, pp. 308–310, July 1958.

[21] N. G. Alexopoulos, D. R. Jackson, and P. B. Katehi, "Criteria for nearly omnidirectional radiation patterns for printed antennas," *IEEE Trans. Antennas Propagat.*, vol. 33, pp. 195–205, Feb. 1985.

[22] N. Engheta and M. M. I. Saadoun, "Novel pseudo chiral or Ω medium and its applications," in *PIERS 1991 Proc.* (Cambridge, MA), July 1–5, 1991, p. 339.

A Pencil-MUSIC Algorithm for Finding Two-Dimensional Angles and Polarizations Using Crossed Dipoles

Yingbo Hua

***Abstract*— We study the problem of finding two-dimensional (2-D) angles of wave arrival and wave polarizations using a uniform rectangular array of crossed dipoles. The method we present in this paper effectively exploits the redundancy in this array via 2-D moving-window smoothing to handle coherent sources and to achieve optimum noise sensitivity. The method combines the computational advantages of the MUSIC and matrix pencil approaches. The method is shown in simulation to be nearly optimum compared with the Cramer–Rao bound.**

I. Introduction

The problem of using a diversely polarized array for wave direction

Manuscript received March 9, 1992; revised September 4, 1992.

The author is with the Department of Electrical and Electronic Engineering, University of Melbourne, Parkville, Victoria 3052, Australia.

IEEE Log Number 9207124.

finding has been addressed very recently in several articles [1]–[5]. The major motivation behind this is the fact that a diversely polarized array can provide higher estimation accuracy than a (corresponding) uniformly polarized array. This observation has been supported by a number of specific algorithms [1]–[4] based on diversely polarized arrays as well as by the analysis of the Cramer–Rao bound [5]. The algorithms that have been developed so far for diversely polarized arrays are specific implementations of the ML (maximum likelihood) method [3], the MUSIC method [4], [5], and the ESPRIT method [1], [2].

While significant progress has been made in understanding and utilizing diversely polarized arrays, there still exist important problems to be solved. In this paper, we will study a uniform rectangular array of crossed dipoles. The importance of this array obviously comes from its simplicity. While the previously mentioned methods are general enough to be applicable to this array, the method we will show is more efficient because it is designed for this array. Specifically, the redundancy of the array is exploited via a moving-window approach to handle coherent sources, and the advantage of MUSIC is enhanced by computing generalized eigenvalues instead of using a search procedure.

In Section II we will formulate the wave model and the outputs of the crossed dipoles. In Section III the pencil–MUSIC algorithm will be developed and discussed. In Section IV we will show the simulation results that compare the performance of the matrix pencil method with the Cramer–Rao bound. It will be seen that nearly optimum performance is achieved by the new method.

II. The Wave Model and Array Output

Assume I narrow-band transverse electromagnetic (TEM) waves impinge upon the array. The ith wave can be expressed by

$$\boldsymbol{e}_i(\boldsymbol{r}, t) = \boldsymbol{e}_{0i}\, a_i(t) \exp(-j\omega t + j\boldsymbol{k}_i \cdot \boldsymbol{r}), \tag{1}$$

where $\boldsymbol{e}_i(\boldsymbol{r}, t)$ denotes the ith electric field at the spatial position $\boldsymbol{r}$, $\boldsymbol{e}_{0i}$ the unit 2-D vector defining the polarization of the ith wave, $a_i(t)$ the (complex) amplitude of the ith wave, which varies slowly with time compared with the frequency ω, and $\boldsymbol{k}_i$ the wave number vector, defined by

$$\boldsymbol{k}_i = -\frac{2\pi}{\lambda}\boldsymbol{u}_{ri}, \tag{2}$$

in which λ is the common wavelength, and $-\boldsymbol{u}_{ri}$ the unit vector defining the traveling direction of the ith wave. $\boldsymbol{k}_i \cdot \boldsymbol{r}$ is the inner product (in the most conventional way) of $\boldsymbol{k}_i$ and $\boldsymbol{r}$.

The polarization vector, $\boldsymbol{e}_{0i}$, can be decomposed as follows:

$$\boldsymbol{e}_{0i} = e_{\phi i}\boldsymbol{u}_{\phi i} + e_{\theta i}\boldsymbol{u}_{\theta i} \tag{3}$$

or, equivalently,

$$\boldsymbol{e}_{0i} = e_{xi}\boldsymbol{u}_x + e_{yi}\boldsymbol{u}_y + e_{zi}\boldsymbol{u}_z, \tag{4}$$

where $\boldsymbol{u}_\phi$, $\boldsymbol{u}_\theta$, $\boldsymbol{u}_x$, $\boldsymbol{u}_y$, and $\boldsymbol{u}_z$ are unit space vectors in azimuth, elevation, x, y, and z directions, respectively. The subscript i indicates the correspondence to the ith wave. $\boldsymbol{u}_\phi$ and $\boldsymbol{u}_\theta$ are related to $\boldsymbol{u}_x$, $\boldsymbol{u}_y$, and $\boldsymbol{u}_z$ as follows:

$$\boldsymbol{u}_{\theta i} = \cos\theta_i \cos\phi_i \boldsymbol{u}_x + \cos\theta_i \sin\phi_i \boldsymbol{u}_y - \sin\theta_i \boldsymbol{u}_z \tag{5}$$

$$\boldsymbol{u}_{\phi i} = -\sin\phi_i \boldsymbol{u}_x + \cos\phi_i \boldsymbol{u}_y. \tag{6}$$

After substituting (5) and (6) into (3) and then comparing (3) and (4), we have

$$e_{xi} = \cos\theta_i \cos\phi_i e_{\theta i} - \sin\phi_i e_{\phi i} \tag{7}$$

$$e_{yi} = \cos\theta_i \sin\phi_i e_{\theta i} + \cos\phi_i e_{\phi i} \tag{8}$$

$$e_{zi} = -\sin\theta_i e_{\theta i}. \tag{9}$$

The polarization of a TEM wave is often specified by two real parameters, $\gamma_i (0 \le \gamma_i \le \pi/2)$ and $\eta_i (-\pi \le \eta_i \le \pi)$, as follows:

$$e_{\theta i} = E \sin\gamma_i \exp(j\eta_i) \tag{10}$$

$$e_{\phi i} = E \cos\gamma_i, \tag{11}$$

where E is an arbitrary (nonzero) complex constant. Clearly, the polarization can be determined by the ratio of $e_{\phi i}$, denoted by λ_i. As implied by (7) and (8), λ_i is a one-to-one linear function of the ratio of e_{xi} to e_{yi}, denoted by t_i, provided the wave directions are known.

The array we consider consists of $M \times N$ crossed dipoles on a uniform rectangular grid with spacing Δx and Δy in the x and y directions. We denote the (complex envelope) outputs of the crossed dipole at $(\Delta xm, \Delta yn)$ by $s_x(t, \Delta xm, \Delta yn)$ and $s_y(t, \Delta xm, \Delta yn)$. Then we define the array output vector:

$$s(t) = \begin{bmatrix} s_x(t) \\ s_y(t) \end{bmatrix}, \tag{12}$$

where

$$s_x(t) = \begin{bmatrix} s_x(t, 0, 0) \\ s_x(t, \Delta x, 0) \\ \cdots \\ s_x(t, (M-1)\Delta x, 0) \\ \cdots \\ \cdots \\ \cdots \\ s_x(t, 0, (N-1)\Delta y) \\ s_x(t, \Delta x, (N-1)\Delta y) \\ \cdots \\ s_x(t, (M-1)\Delta x, (N-1)\Delta y) \end{bmatrix} \tag{13}$$

and $s_y(t)$ is similarly defined. Clearly, $s_x(t)$ consists of the outputs of the dipoles in the x direction, and $s_y(t)$ the outputs of the dipoles in the y direction. Then it can be shown that

$$\boldsymbol{s}(t) = \begin{bmatrix} \boldsymbol{K}_{pq}\boldsymbol{E}_x\boldsymbol{a}(t) \\ \boldsymbol{K}_{pq}\boldsymbol{E}_y\boldsymbol{a}(t) \end{bmatrix}, \tag{14}$$

where

$$\boldsymbol{a}(t) = [a_1(t), a_2(t), \cdots, \cdots, a_I(t)]^T \tag{15}$$

$$\boldsymbol{E}_x = \operatorname{diag}[e_{x1}, e_{x2}, \cdots, e_{xI}] \tag{16}$$

$$\boldsymbol{E}_y = \operatorname{diag}[e_{y1}, e_{y2}, \cdots, e_{yI}] \tag{17}$$

$$\boldsymbol{K}_{pq} = [\boldsymbol{p}_1 \otimes \boldsymbol{q}_1, \boldsymbol{p}_2 \otimes \boldsymbol{q}_2, \cdots, \boldsymbol{p}_I \otimes \boldsymbol{q}_I] \tag{18}$$

$$\boldsymbol{p}_i = [1, p_i, \cdots, \cdots, p_i^{M-1}]^T \tag{19}$$

$$\boldsymbol{q}_i = [1, q_i, \cdots, \cdots, q_i^{N-1}]^T \tag{20}$$

$$p_i = \exp\left(-j\frac{2\pi}{\lambda}\Delta x \cos\alpha_i\right) \tag{21}$$

$$q_i = \exp\left(-j\frac{2\pi}{\lambda}\Delta y \cos\beta_i\right). \tag{22}$$

The superscript ^{T} denotes transpose, and $\otimes$ the Kronecker product, i.e.,

$$\boldsymbol{p}_i \otimes \boldsymbol{q}_i = \begin{bmatrix} \boldsymbol{p}_i \\ \boldsymbol{p}_i q_i \\ \cdots \\ \cdots \\ \boldsymbol{p}_i q_i^{N-1} \end{bmatrix} \tag{23}$$

α_i and β_i are angles of the ith wave with the x and y axes. The one-to-one function between (α_i, β_i) and (ϕ_i, θ_i) can be easily derived. The above compact expressions for the array outputs are very useful for developing a pencil–MUSIC algorithm for finding the wave directions and polarizations, as will be shown next.

III. The Pencil–MUSIC Algorithm

We start with the array output covariance matrix, which is defined as

$$\boldsymbol{R}_s = \mathrm{E}\left\{ \begin{bmatrix} s_x(t) \\ s_y(t) \end{bmatrix} \begin{bmatrix} s_x(t) \\ s_y(t) \end{bmatrix}^* \right\} \tag{24}$$

where $\mathrm{E}\{\cdot\}$ denotes the expectation, and the asterisk the conjugate transpose. Using (14), it follows that

$$\boldsymbol{R}_s = \begin{bmatrix} \boldsymbol{K}_{pq}\boldsymbol{E}_x \\ \boldsymbol{K}_{pq}\boldsymbol{E}_y \end{bmatrix} \boldsymbol{R}_a \begin{bmatrix} \boldsymbol{K}_{pq}\boldsymbol{E}_x \\ \boldsymbol{K}_{pq}\boldsymbol{E}_y \end{bmatrix}^*, \tag{25}$$

where $\boldsymbol{R}_a = \mathrm{E}\{\boldsymbol{a}(t)\boldsymbol{a}(t)^*\}$. For coherent waves for which rank $(\boldsymbol{R}_a)$ is less than the number of waves, the covariance matrix $\boldsymbol{R}_s$ is ill conditioned. Hence, we cannot expect the performance of any methods (such as [1] and [2]) based on the eigendecomposition of $\boldsymbol{R}_s$ to be good in the coherent case. In order to overcome the coherent case and increase the noise robustness, we exploit the redundancy in the 2-D array of uniformly distributed crossed dipoles. For a uniform linear array problem, the redundancy was effectively exploited in [11] by averaging subcovariance matrices corresponding to subarrays. The following represents an extension of the previous work from a uniform 1-D array to a uniform 2-D array. We first define

$$\boldsymbol{R}_s = \begin{bmatrix} \boldsymbol{R}(1,1) & \boldsymbol{R}(1,2) \\ \boldsymbol{R}(2,1) & \boldsymbol{R}(2,2) \end{bmatrix}, \tag{26}$$

where each submatrix, $\boldsymbol{R}(i, j)$, has the dimension $MN \times MN$. Then we write

$$\boldsymbol{R}(i,j) = \begin{bmatrix} \boldsymbol{R}_{0,0}(i,j) & \boldsymbol{R}_{0,1}(i,j) & \cdots & \cdots & \boldsymbol{R}_{0,N-1}(i,j) \\ \boldsymbol{R}_{1,0}(i,j) & \boldsymbol{R}_{1,1}(i,j) & \cdots & \cdots & \boldsymbol{R}_{1,N-1}(i,j) \\ \cdots & \cdots & \cdots & \cdots & \cdots \\ \cdots & \cdots & \cdots & \cdots & \cdots \\ \boldsymbol{R}_{N-1,0}(i,j) & \boldsymbol{R}_{N-1,1}(i,j) & \cdots & \cdots & \boldsymbol{R}_{N-1,N-1}(i,j) \end{bmatrix} \tag{27}$$

where $\boldsymbol{R}_{n1,n2}(i, j)$ is the $(n1, n2)$th $M \times M$ submatrix and is expressed as

$$\boldsymbol{R}_{n1,n2}(i,j) = \begin{bmatrix} r_{0,0}(n1,n2,i,j) & r_{0,1}(n1,n2,i,j) & \cdots & \cdots & r_{0,M-1}(n1,n2,i,j) \\ r_{1,0}(n1,n2,i,j) & r_{1,1}(n1,n2,i,j) & \cdots & \cdots & r_{1,M-1}(n1,n2,i,j) \\ \cdots & \cdots & \cdots & \cdots & \cdots \\ \cdots & \cdots & \cdots & \cdots & \cdots \\ r_{M-1,0}(n1,n2,i,j) & r_{M-1,1}(n1,n2,i,j) & \cdots & \cdots & r_{M-1,M-1}(n1,n2,i,j) \end{bmatrix} \tag{28}$$

A. Enhanced Matrix

Let J and K be two positive integers less than M and N respectively. We now define the $2JK \times 2JK$ enhanced matrix (via averaging subcovariance matrices):

$$\overline{\boldsymbol{R}}_s = \begin{bmatrix} \overline{\boldsymbol{R}}(1,1) & \overline{\boldsymbol{R}}(1,2) \\ \overline{\boldsymbol{R}}(2,1) & \overline{\boldsymbol{R}}(2,2) \end{bmatrix} \tag{29}$$

where $\overline{\boldsymbol{R}}(i, j)$ is a $(K \times K)$ block matrix defined by

$$\overline{\boldsymbol{R}}(i,j) = \sum_{k=0}^{N-K} \begin{bmatrix} \overline{\boldsymbol{R}}_{k,k}(i,j) & \overline{\boldsymbol{R}}_{k,k+1}(i,j) & \cdots & \cdots & \overline{\boldsymbol{R}}_{k,k+K-1}(i,j) \\ \overline{\boldsymbol{R}}_{k+1,k}(i,j) & \overline{\boldsymbol{R}}_{k+1,k+1}(i,j) & \cdots & \cdots & \overline{\boldsymbol{R}}_{k+1,k+K-1}(i,j) \\ \cdots & \cdots & \cdots & \cdots & \cdots \\ \cdots & \cdots & \cdots & \cdots & \cdots \\ \overline{\boldsymbol{R}}_{k+K-1,k}(i,j) & \overline{\boldsymbol{R}}_{k+K-1,k+1}(i,j) & \cdots & \cdots & \overline{\boldsymbol{R}}_{k+K-1,k+K-1}(i,j) \end{bmatrix} \tag{30}$$

in which the $(k1, k2)$th block, $\overline{\boldsymbol{R}}_{k1,k2}(i, j)$, has the dimension $J \times J$ and is defined by

$$\overline{\boldsymbol{R}}_{k1,k2}(i',j') = \sum_{j=0}^{M-J} \begin{bmatrix} r_{j,j}(k1,k2,i',j') & r_{j,j+1}(k1,k2,i',j') & \cdots & \cdots & r_{j,j+J-1}(k1,k2,i',j') \\ r_{j+1,j}(k1,k2,i',j') & r_{j+1,j+1}(k1,k2,i',j') & \cdots & \cdots & r_{j+1,j+J-1}(k1,k2,i',j') \\ \cdots & \cdots & \cdots & \cdots & \cdots \\ \cdots & \cdots & \cdots & \cdots & \cdots \\ r_{j+J-1,j}(k1,k2,i',j') & r_{j+J-1,j+1}(k1,k2,i',j') & \cdots & \cdots & r_{j+J-1,j+J-1}(k1,k2,i',j') \end{bmatrix} \tag{31}$$

Note that $\overline{\boldsymbol{R}}(i, j)$ is a smoothed version (sum) of the $(K \times K)$ block submatrices along the diagonal axis of $\boldsymbol{R}(i, j)$, and $\overline{\boldsymbol{R}}_{k1,k2}(i, j)$ is a smoothed version (sum) of the $J \times J$ submatrices along the diagonal axis of $\boldsymbol{R}_{k1,k2}(i, j)$. Therefore, it is not necessary to compute the whole covariance matrix $\boldsymbol{R}_s$ of the (larger) dimension $2MN \times 2MN$ to obtain the enhanced matrix of the (smaller) dimension $2JK \times 2JK$.

B. Structure of Enhanced Matrix

With the above definitions, we now discuss the inherent structure of the enhanced matrix. Based on (25) and (16)–(23), we know that the $(m1, m2)$th element of $\boldsymbol{R}_{n1,n2}(i, j)$ is

$$r_{m1,m2}(n1, n2, i, j) = [p_1^{m1} q_1^{n1}, \cdots, p_I^{m1} q_I^{n1}]\, \boldsymbol{R}_a(i, j) [p_1^{m2} q_1^{n2}, \cdots, p_I^{m2} q_I^{n2}]^*, \quad (32)$$

where

$$\boldsymbol{R}_a(i, j) = \begin{cases} \boldsymbol{E}_x \boldsymbol{R}_a \boldsymbol{E}_x^* & (i, j) = (1, 1) \\ \boldsymbol{E}_x \boldsymbol{R}_a \boldsymbol{E}_y^* & (i, j) = (1, 2) \\ \boldsymbol{E}_y \boldsymbol{R}_a \boldsymbol{E}_x^* & (i, j) = (2, 1) \\ \boldsymbol{E}_y \boldsymbol{R}_a \boldsymbol{E}_y^* & (i, j) = (2, 2). \end{cases} \quad (33)$$

Using (32) and (33) in (29)–(31), one can verify the following:

$$\overline{\boldsymbol{R}}_{s3} = \begin{bmatrix} \boldsymbol{K}'_{pq} \boldsymbol{E}_x \\ \boldsymbol{K}'_{pq} \boldsymbol{E}_y \end{bmatrix} \overline{\boldsymbol{R}}_a \begin{bmatrix} \boldsymbol{K}'_{pq} \boldsymbol{E}_x \\ \boldsymbol{K}'_{pq} \boldsymbol{E}_y \end{bmatrix}^* \quad (34)$$

where

$$\boldsymbol{K}'_{pq} = [\boldsymbol{p}'_1 \otimes \boldsymbol{q}'_1, \boldsymbol{p}'_2 \otimes \boldsymbol{q}'_2, \cdots, \boldsymbol{p}'_I \otimes \boldsymbol{q}'_I] \quad (35)$$

$$\boldsymbol{p}'_i = [1, p_i, \cdots, \cdots, p_i^{J-1}]^T \quad (36)$$

$$\boldsymbol{q}'_i = [1, q_i, \cdots, \cdots, q_i^{K-1}]^T \quad (37)$$

$$\overline{\boldsymbol{R}}_a = \sum_{j=0}^{M-J} \sum_{k=0}^{N-K} \boldsymbol{P}^j \boldsymbol{Q}^k \boldsymbol{R}_a \boldsymbol{Q}^{*k} \boldsymbol{P}^{*j} \quad (38)$$

$$\boldsymbol{P} = \text{diag}\,(p_1, p_2, \cdots, p_I) \quad (39)$$

$$\boldsymbol{Q} = \text{diag}\,(q_1, q_2, \cdots, q_I). \quad (40)$$

C. Conditions on J and K

We now derive the conditions on J and K under which $\overline{\boldsymbol{R}}_s$ is always of the rank I (the desired rank [9]). First, we can see from (34) (the necessary condition) that if rank $(\overline{\boldsymbol{R}}_a) = I$ and rank $(\boldsymbol{K}'_{pq}) = I$, then rank $(\overline{\boldsymbol{R}}_s) = I$. This condition is also a necessary condition when $\boldsymbol{E}_x = \boldsymbol{E}_y$.

The least favourable case for $\overline{\boldsymbol{R}}_a$ to have the rank I is when $\boldsymbol{R}_a$ has the rank 1 (e.g., all waves are perfectly correlated). For such case, we can write

$$\boldsymbol{R}_a = \phi \phi^*, \quad (41)$$

where ϕ is an $I \times 1$ vector with no element equal to 0. (A zero element in ϕ would mean that there are fewer than I waves impinging on the array.) Then we can write $\overline{\boldsymbol{R}}_a$ from (38) into

$$\overline{\boldsymbol{R}}_a = \Phi \Phi^*, \quad (42)$$

where

$$\Phi = [\phi, \boldsymbol{P}\phi, \cdots, \boldsymbol{P}^{M-J}\phi, \boldsymbol{Q}\phi, \boldsymbol{P}\boldsymbol{Q}\phi, \cdots, \boldsymbol{P}^{M-J}\boldsymbol{Q}\phi, \cdots, \cdots, \boldsymbol{Q}^{N-K}\phi, \boldsymbol{P}\boldsymbol{Q}^{N-K}\phi, \cdots, \boldsymbol{P}^{M-J}\boldsymbol{Q}^{N-K}\phi] = \Phi_0 \boldsymbol{K}''^T_{pq}, \quad (43)$$

in which

$$\Phi_0 = \text{diag}\,(\phi) \quad (44)$$

$$\boldsymbol{K}''_{pq} = [\boldsymbol{p}''_1 \otimes \boldsymbol{q}''_1, \boldsymbol{p}''_2 \otimes \boldsymbol{q}''_2, \cdots, \boldsymbol{p}''_I \otimes \boldsymbol{p}''_I] \quad (45)$$

$$\boldsymbol{p}''_i = [1, p_i, \cdots, \cdots, p_i^{M-K}]^T \quad (46)$$

$$\boldsymbol{q}''_i = [1, q_i, \cdots, \cdots, q_i^{N-L}]^T \quad (47)$$

It can be shown that provided (p_i, q_i) for $i = 1, 2, \cdots, I$ are distinct pairs (as they should be), $\boldsymbol{K}''_{pq}$ has the rank I if the following sufficient condition is satisfied:

$$\begin{cases} I \le M - J + 1 \\ I \le N - K + 1 \end{cases} \quad (48)$$

The above condition is also necessary in the sense that $\boldsymbol{K}''_{pq}$ can have rank less than I if the condition is not satisfied.

Given Φ_0 and $\boldsymbol{K}''_{pq}$ both of the full rank I, Φ is of the full rank, and so is $\overline{\boldsymbol{R}}_a$. Therefore, (48) is sufficient (and somewhat necessary) for $\overline{\boldsymbol{R}}_a$ to be of rank I regardless of the wave coherency or polarization.

Following the discussion on $\boldsymbol{K}''_{pq}$, we know that $\boldsymbol{K}'_{pq}$ has the rank I under the sufficient (and somewhat necessary) condition

$$\begin{cases} I \le J \\ I \le K. \end{cases} \quad (49)$$

Therefore, it follows that, under the conditions of (48) and (49), the enhanced matrix $\overline{\boldsymbol{R}}_s$ is always of the desired rank I.

D. MUSIC

Having established the enhanced matrix $\overline{\boldsymbol{R}}_s$ and understood its internal structure, one can follow a standard MUSIC approach and derive the following MUSIC algorithm.

- Compute the estimated covariance matrix $\hat{\overline{\boldsymbol{R}}}_s$ (via averaging over time or snapshots). Considering an additive white noise in the array output, we can write (for a large number of snapshots, a large number of crossed dipoles, or high SNR)

$$\hat{\overline{\boldsymbol{R}}}_s \approx \overline{\boldsymbol{R}}_s + 2\sigma^2 \boldsymbol{I}, \quad (50)$$

  where $2\sigma^2$ is the noise variance, and $\boldsymbol{I}$ the identity matrix.
- Compute the eigendecomposition:

$$\hat{\overline{\boldsymbol{R}}}_s = \hat{\boldsymbol{U}} \hat{\Lambda} \hat{\boldsymbol{U}}^*, \quad (51)$$

  where

$$\hat{\Lambda} = \text{diag}\,(\hat{\lambda}_1, \hat{\lambda}_2, \cdots, \hat{\lambda}_I, \hat{\lambda}_{I+1}, \cdots, \hat{\lambda}_{2JK}) \quad (52)$$

$$\hat{\boldsymbol{U}} = [\hat{\boldsymbol{u}}_1, \hat{\boldsymbol{u}}_2, \cdots, \hat{\boldsymbol{u}}_I, \hat{\boldsymbol{u}}_{I+1}, \cdots, \hat{\boldsymbol{u}}_{2JK}]. \quad (53)$$

  Note that asymptotically $\lambda_1 > \lambda_2 > \cdots > \lambda_I > \lambda_{I+1} = \cdots = \lambda_{2JK} = 2\sigma^2$. Using this property, the number of waves can be found. More sophisticated methods for the detection problem are available via [12].
- Search for I peak positions $\{(\hat{\theta}_i, \hat{\phi}_i, \hat{\gamma}_i, \hat{\eta}_i)$ for $i = 1, 2, \cdots, I\}$ of the 4-D spectrum:

$$P(\theta, \phi, \gamma, \eta) = \frac{1}{\sum_{j=I+1}^{2JK} |\hat{\boldsymbol{u}}_{j1}^* (\boldsymbol{p}' \otimes \boldsymbol{q}') t + \hat{\boldsymbol{u}}_{j2}^* (\boldsymbol{p}' \otimes \boldsymbol{q}')|^2} \quad (54)$$

  where $\hat{\boldsymbol{u}}_{j1}$ and $\hat{\boldsymbol{u}}_{j2}$ are the top and bottom $JK \times 1$ subvectors of $\hat{\boldsymbol{u}}_j$ respectively. Note that t is a complex function of γ and η and that $\boldsymbol{p}'$ and $\boldsymbol{q}'$ are functions of θ and ϕ (as defined before but with the subscript i dropped). Also note that the search can be reduced to a 2-D search problem. This is because the MUSIC

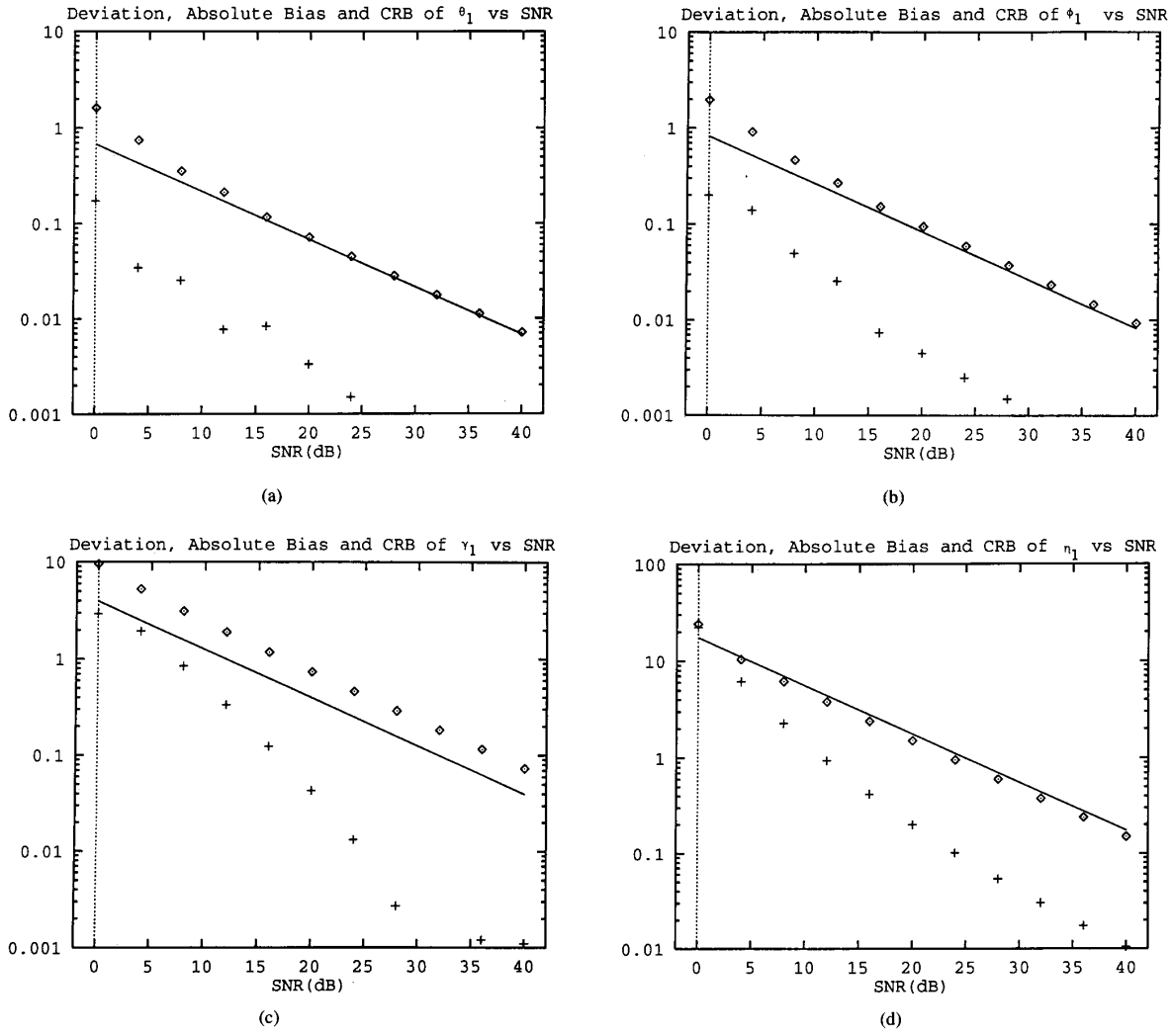

Fig. 1. 200-run sample deviations and biases (in absolute value) of estimatedangles and polarizations compared with the Cramer–Rao bound. The verticalscales are in degrees. "◊" represents the deviation, "+" thebias, and the straight lines are the CRB: (a) for θ_1; (b) forϕ_1; (c) for γ_1; (d) for η_1.

spectrum $P(\theta, \phi, \gamma, \eta)$ is a quadratic function of t, and t is a linear function of the polarization constant λ. This means that the optimum λ (then optimum t or optimum γ and η) can be derived as a closed-form function of θ and ϕ. With the closed-form function substituted for t in (54), the MUSIC spectrum becomes 2-D. A similar approach was used in [4].

E. Pencil–MUSIC

While the MUSIC algorithm is much more efficient than the ML method, further improvement of computation can be made by solving a matrix pencil problem, instead of a searching procedure, as shown below.

- Follow the steps in the MUSIC algorithm until the I principal eigenvectors $\hat{\boldsymbol{u}}_i$ for $i = 1, 2, \cdots, I$ are obtained.
- Let $\hat{U}_s = [\hat{\boldsymbol{u}}_1, \hat{\boldsymbol{u}}_2, \cdots, \hat{\boldsymbol{u}}_I] = \begin{bmatrix} \hat{U}_{s1} \\ \hat{U}_{s2} \end{bmatrix}$, where the two submatrices $\hat{U}_{s1}$ and $\hat{U}_{s2}$ have the dimension $JK \times I$.
- From the following matrix pencils and compute their generalized eigenvalues):

$$\hat{U}_{s1} - t\hat{U}_{s2}$$

$$\hat{U}_{p1} - p\hat{U}_{p2}$$

$$\hat{U}_{q1} - q\hat{U}_{q2}$$

where

$$\hat{U}_{p1} = \begin{bmatrix} \hat{U}_{s1} \text{ with its 1st, } (1+J)\text{th}, \cdots, \\ (1+(K-1)J)\text{th rows deleted} \\ \hat{U}_{s2} \text{ with its 1st, } (1+J)\text{th}, \cdots, \\ (1+(K-1)J)\text{th rows deleted} \end{bmatrix}$$

$$\hat{U}_{p2} = \begin{bmatrix} \hat{U}_{s1} \text{ with its } J\text{th}, 2J\text{th}, \cdots, KJ\text{th rows deleted} \\ \hat{U}_{s2} \text{ with its } J\text{th}, 2J\text{th}, \cdots, KJ\text{th rows deleted} \end{bmatrix}$$

$$\hat{U}_{q1} = \begin{bmatrix} \hat{U}_{s1} \text{ with its first } J \text{ rows deleted} \\ \hat{U}_{s2} \text{ with its first } J \text{ rows deleted} \end{bmatrix}$$

$$\hat{U}_{q2} = \begin{bmatrix} \hat{U}_{s1} \text{ with its last } J \text{ rows deleted} \\ \hat{U}_{s2} \text{ with its last } J \text{ rows deleted} \end{bmatrix}.$$

To justify the above matrix manipulations, we first note that in the noiseless case or asymptoptically, the range of U_s is the same as that of $\overline{R}_s$, i.e.,

$$U_s = \begin{bmatrix} K'_{pq} E_x \\ K'_{pq} E_y \end{bmatrix} Q, \tag{55}$$

where Q is a nonsingular $I \times I$ matrix. Then it follows that

$$U_{s1} - tU_{s2} = K'_{pq}(E_x - tE_y)Q, \tag{56}$$

which implies that t_i for $i = 1, 2, \cdots, I$ are the generalized eigenvalues (rank reducing numbers [6]) of the matrix pencil U_{s1}–tU_{s2}. Considering the second and third matrix pencils U_{p1}–pU_{p2} and U_{q1}–qU_{q2}, we write

$$U_{p1}\text{–}pU_{p2} = K'_{pq,\,p}(P - pI)Q \tag{57}$$

$$U_{q1}\text{–}qU_{q2} = K'_{pq,\,q}(Q - qI)Q, \tag{58}$$

where

$$K'_{pq,\,p} = [p'''_1 \otimes q'_1, p'''_2 \otimes q'_2, \cdots, p'''_I \otimes q'_I] \tag{59}$$

$$K'_{pq,\,q} = [p'_1 \otimes q'''_1, p'_2 \otimes q'''_2, \cdots, p'_I \otimes q'''_I] \tag{60}$$

$$p'''_i = [1, p_i, \cdots, \cdots, p_i^{J-2}]^T \tag{61}$$

$$q'''_i = [1, q_i, \cdots, \cdots, q_i^{K-2}]^T. \tag{62}$$

If condition (49) is made more strict by assuming

$$\begin{cases} I \le J - 1 \\ I \le K - 1, \end{cases} \tag{63}$$

then both $K'_{pq,\,p}$ and $K'_{pq,\,q}$ are of the full rank I. Then it follows from (57) and (58) that p_i for $i = 1, 2, \cdots, I$ and q_i for $i = 1, 2, \cdots, I$ are the generalized eigenvalues (rank reducing numbers) of the matrix pencils U_{p1}–pU_{p2} and U_{q1}–qU_{q2}, respectively. Several algorithms for computing the generalized eigenvalues are available in [13]. A noise robust version is called TLS-ESPRIT [10].

- Having obtained the estimates of t_i for $i = 1, 2, \cdots, I$, p_i for $i = 1, 2, \cdots, I$, and q_i for $i = 1, 2, \cdots, I$, we need to have them correctly paired. They can be paired by maximizing the function $P(\theta, \phi, \gamma, \eta)$ with respect to the available t_i's, p_i's, and q_i's. Note that this maximization can be reduced to 2-D, as discussed before. The 2-D pairing can be made by selecting the I largest values of the MUSIC spectrum computed for all I^2 possible pairs between the p_i's and q_i's. (Note that the pairing between the t_i's and (p_i, q_i)'s can be similarly done). Due to noise, this method does not guarantee that each p_i has a mate of q_i and vice versa. Alternatively, one can do the following. A best mate is chosen from I q_i's for p_1, and then a best mate from the remaining $I-1$ q_i's for p_2, and so on. The latter method (for pairing p_i's and q_i's) requires $(I(I+1))/2 - 1$ computations of the MUSIC spectrum, as opposed to I^2 for the former one.
- Having found and paired (t_i, p_i, q_i) for $i = 1, 2, \cdots, I$, the wave angles (θ_i, ϕ_i) and polarizations (γ_i, η_i) can be straightforwardly computed according to the discussions in Section II.

IV. Simulations

To illustrate the noise performance, we assume a 20×20 square array of crossed dipoles with the spacing between crossed dipoles being a quarter of the wavelength and two TEM waves impinging on the array with the angles $(\theta_1, \phi_1) = (40°, 40°)$ and $(\theta_2, \phi_2) = (45°, 45°)$ and polarizations $(\gamma_1, \eta_1) = (45°, -90°)$ and $(\gamma_2, \eta_2) = (45°, 90°)$. The first wave is counterclockwise circularly polarized, and the second is clockwise. The complex wave amplitudes are equal to 1 with zero phase; i.e., $a_1(t) = a_2(t) = 1$. We used one-snapshot outputs of the array for the simulation. White Gaussian noise was added to the array output. Two hundred independent runs were executed to compute sample means and sample deviations of the estimated angles and polarizations. The two integers J and K were chosen to be 3, which is the smallest number satisfying the conditions of (48) and (63). Increasing J and K would increase the computations. The sample deviations and biases of the estimated θ_1, ϕ_1, γ_1, and η_1 (all in degrees) are shown in parts (a)–(d) of Fig. 1 together with the associated Cramer–Rao bounds. The computation of the Cramer–Rao bound assumes that the noise is complex white Gaussian with zero mean and variance $2\sigma^2$, and the unknown parameters are $\{\theta_i, \phi_i, \gamma_i, \eta_i, |a_i(t)|, \arg(a_i(t))$; for $i = 1, 2, \cdots, I\}$. (Note that the amplitudes are chosen to be unknown deterministic because only one snap-shot case is considered here. For large numbers of snap shots, the random amplitudes should be a better model, i.e., provide tighter CRB. Also note that the square root of the bound on variance is used as the bound on deviation.) It can be seen from these figures that the deviations are very close to the bound until the SNR is zero dB. The SNR is defined as $-10\log_{10}(2\sigma^2)$. The fact that the biases are much smaller than the deviations, as shown in these figures, means that the Cramer–Rao bound must be a good approximation of the *exact* lower bound on estimation variation (or deviation) [14]. The performance of the method broke down quickly when the SNR was lower than zero dB. The sample deviations and biases for the second wave are similar to those for the first wave and hence are omitted here.

V. Conclusions

We have studied the problem of estimating 2-D angles and polarizations based on a uniform rectangular array of crossed dipoles. A pencil–MUSIC algorithm has been developed. This algorithm represents a generalization of the matrix pencil approach [6], [7] and the moving-window smoothing approach [11], and a refinement of MUSIC. The method can effectively handle coherent sources. Our simulation has shown that this method has nearly optimum performance compared with the Cramer–Rao bound.

Acknowledgment

The reviewers' comments have contributed to the present form of presentation.

References

[1] J. Li and R. T. Compton, Jr., "Angle and polarization estimation using ESPRIT with a polarization sensitive array," *IEEE Trans. Antennas Propagat.*, vol. 39, pp. 1376–1383, Sept. 1991.

[2] J. Li and R. T. Compton, Jr., "Angle estimation using a polarization sensitive array," *IEEE Trans. Antennas Propagat.*, vol. 39, pp. 1539–1543, Oct. 1991.

[3] I. Ziskind and M. Wax, "Maximum likelihood localization of diversely polarized sources by simulated annealing," *IEEE Trans. Antennas Propagat.*, vol. 38, pp. 1111–1114, July 1990.

[4] E. Ferrara, Jr., and T. M. Parks, "Direction finding with an array of antennas having diversely polarizations," *IEEE Trans. Antennas Propagat.*, vol. 31, pp. 231–236, Mar. 1983.

[5] A. J. Weiss and B. Friedlander, "Performance analysis of diversly polarized antenna arrays," *IEEE Trans. Signal Process.*, vol. 39, pp. 1589–1603, July 1991.
[6] Y. Hua and T. K. Sarkar, "Generalized pencil-of-functions method for extracting the poles of an electromagnetic system from its transient response," *IEEE Trans. Antennas Propagat.*, vol. 37, pp. 229–234, Feb. 1989.
[7] Y. Hua and T. K. Sarkar, "Matrix pencil method for estimating parameters of exponentially damped/undamped sinusoids in noise," *IEEE Trans. Acoust., Speech, Signal Process.*, vol. 38, pp. 814–824, May 1990.
[8] Y. Hua, "Estimating two-dimensional frequencies by matrix enhancement and matrix pencil," in *Proc. IEEE ICASSP91* (Toronto, Canada), May 1991.
[9] R. O. Schmidt, "A signal subspace approach to multiple emitter location and spectral estimation," Ph.D. dissertation, Stanford University, CA, 1981.
[10] R. H. Roy, "ESPRIT—Estimation of signal parameters via rotational invariance techniques," Ph.D. dissertation, Stanford University, CA, 1987.
[11] T. J. Shan, M. Wax, and T. Kailath, "On spatial smoothing for direction-of-arrival estimation of coherent signals," *IEEE Trans. Acoust., Speech, Signal Process.*, vol. 33, pp. 806–811, Aug. 1985.
[12] W. Chen, K. M. Wong, and J. P. Reilly, "Detection of the number of signals: a predicted eigen-threshold approach," *IEEE Trans. Signal Process.*, vol. 39, pp. 1088–1098, May 1991.
[13] Y. Hua and T. K. Sarkar, "On SVD for estimating generalized eigenvalues of matrix pencil in noise," *IEEE Trans. Signal Process.*, vol. 39, pp. 892–900, Apr. 1991.
[14] H. L. Van Trees, *Detection, Estimation and Modulation Theory, Part I.* New York: Wiley, 1968.
[15] R. Kumaresan and D. W. Tufts, "Estimating the angles of arrival of multiple plane waves," *IEEE Trans. Aerospace Electron. Syst.*, vol. 19, pp. 134–139, Jan. 1983.

The RCS of a Microstrip Dipole Deduced from an Expansion of Pole Singularities

George W. Hanson and Dennis P. Nyquist

Abstract—**The singularity expansion method (SEM) is applied to the steady-state analysis of plane wave scattering from microstrip dipoles. The current induced on the antenna is expanded in a series of natural modes, where the amplitude of each term in the expansion is expressed as a coupling coefficient weighted by a simple frequency pole. Natural modes occur at pole singularities of the antenna current in the complex frequency plane, and are found by a numerical root search of a homogeneous matrix equation. This formulation results in an accurate and efficient calculation of the radar cross section (RCS) of microstrip dipoles which exhibit some appreciable resonant characteristics, where it is found that the current resonance dominates the response of the antenna. The SEM applied here yields good physical insight into the scattering behavior of such antennas. Results obtained with the SEM analysis are compared with a full-wave method of moments (MoM) solution.**

I. Introduction

Microstrip antennas frequently find application on vehicles since they are lightweight, conformal, and relatively inexpensive. Because they are often found on the exterior of vehicles, determination of their RCS is important. While the radiation and input properties of microstrip dipoles have been studied extensively, their scattering properties have only recently been addressed [1], although scattering from microstrip patch antennas has been considered by several authors [2]–[4].

Manuscript received April 24, 1992; revised November 2, 1992.

G. W. Hanson is with the Department of Electrical Engineering and Computer Science, University of Wisconsin-Milwaukee, Milwaukee, WI 53201.
D. P. Nyquist is with the Department of Electrical Engineering, Michigan State University, East Lansing, MI 48824.

IEEE Log Number 9207125.

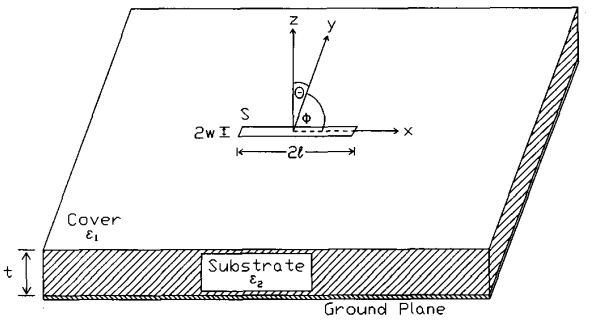

Fig. 1. Microstrip dipole geometry.

In this work, the RCS of a microstrip dipole based upon a pole-singularity expansion (PSE) of the antenna current is presented. The current expansion is formed as a series of natural modes, where a "natural mode" refers to a complex resonant frequency and the associated current distribution. The amplitude of each term in the series is given by a coupling coefficient weighted by a simple frequency pole. The coupling coefficients, which are overlap integrals between the natural modes of the antenna and the incident excitation, are similar in form to the "class 1" coupling coefficients used in the well-known singularity expansion method (SEM) [5]–[7], although their evaluation is complicated by the presence of the Green function for the microstrip environment.

The RCS of several microstrip dipole configurations is presented, and results are compared with a full-wave MoM solution. The efficiency and accuracy of this method, as well as the range of its applicability, are discussed. It is found that the PSE method provides good physical insight into the dominant scattering phenomena for dipoles printed on generally lossy thin substrates.

II. Theory

The geometry of a microstrip dipole is shown in Fig. 1. The dielectric cover and substrate, regions 1 and 2, respectively, are assumed to be linear, isotropic, and homogeneous, with relative permitivity ϵ_{ri} and loss tangent $\tan\delta_i$ for the ith region. The wave number and intrinsic impedance in each region are $k_i = \sqrt{\epsilon_i}k_0$ and $\eta_i = \eta_0/\sqrt{\epsilon_i}$, where (k_0, η_0) are their free-space counterparts. For the results presented here the cover region is assumed to be free space, and the substrate is nonmagnetic.

The electric field in the cover maintained by currents in the cover is

$$\vec{E}_1(\vec{r}) = \frac{-j\eta_1}{k_1}\int_S \overleftrightarrow{G}^e(\vec{r} \mid \vec{r}') \cdot \vec{K}(\vec{r}')\, dS', \qquad (1)$$

where $\overleftrightarrow{G}^e(\vec{r} \mid \vec{r}')$ is an appropriate electric dyadic Green function for the layered geometry [8]. Scattering from a microstrip dipole is deduced from the EFIE

$$-\frac{j\eta_1}{k_1}\hat{t} \cdot \int_S \overleftrightarrow{G}^e(\vec{r} \mid \vec{r}') \cdot \vec{K}(\vec{r}')\, dS' = -\hat{t} \cdot \vec{E}_1^i(\vec{r}) \ldots \forall \vec{r} \in S, \quad (2)$$